Tensor Components in Three Pulse Vibrational Echoes of a Rigid Dipeptide

Jens Dreyer,[†,*] Andrew M. Moran, and Shaul Mukamel

Department of Chemistry, Department of Physics and Astronomy, University of Rochester, Rochester, NY 14627-0216, USA

Received April 14, 2003

The effects of different polarization conditions on vibrational echo signals are systematically explored for the rigid cyclic dipeptide 2,5-diazabicyclo[2.2.2]octane-3,6-dione. An anharmonic vibrational Hamiltonian is constructed by computing energy derivatives to fourth order using density functional theory. Molecular frame transition dipole orientations are then used to calculate polarization dependent orientational factors corresponding to various Liouville space pathways. Enhancement and elimination of specific peaks in two-dimensional correlation plots is accomplished by identifying appropriate pulse configurations.

Key Words : Vibrational echo, Dipeptide

Introduction

Two-dimensional IR spectroscopy provides new insight into structural dynamics of molecular systems with femtosecond time resolution.[1,2] Cross peaks in 2D correlation plots directly reveal the anharmonic coupling between different vibrational modes in the molecule. Frequencies of these peaks represent the coherent evolution of the system between interactions with the laser pulses. The intensities depend on the mutual orientations of the transition dipole moments of the respective vibrational transitions in the molecular frame as well as on the orientations of the IR pulses in the laboratory frame.[3,4] Structural characteristics of the molecule are therefore represented by peak positions and intensities.

For pairs of modes with frequency differences that are comparable to the linewidth, the extraction of structural information may be restricted by the overlap of intense diagonal peaks with the desired cross peaks. For this reason, techniques to eliminate the diagonal peaks by taking advantage of the polarization dependence of the nonlinear IR signal have been developed.[3] The ensemble averaged formula for the third order orientational factor given in Reference 3 assumes that the transition dipoles are fixed in the molecular frame during the course of an experiment (~1-2 ps). Although molecular rotation is likely to be negligible on this time scale, contributions resulting from changes in internal degrees of freedom can be significant for flexible systems. This formula is therefore most appropriate for relatively rigid structures.

Structural parameters of peptides have been determined by measuring the polarization dependence of 2D IR spectra using double-resonance[5,6] as well as heterodyned[7-9] techniques. Resolution enhancement of the structurally sensitive cross peaks can be achieved by subtracting different tensor components to yield spectra without diagonal peaks. However, this approach is complicated by the need to normalize spectra obtained in two different measurements with respect to each other, and may result in imperfectly subtracted diagonal peaks due to inequivalent contributions from reorientational dynamics.[4,8] These difficulties are avoided by applying specific polarization conditions in single measurements that are equivalent to linear combinations of certain tensor components.[8]

In order to analyze 2D IR spectra and to design new experiments independent simulations of the spectra are necessary. To this end, we have developed a new approach to predict coherent third order spectroscopic signals from first principles.[10-12] We generate an anharmonic force-field up to fourth-order as well as dipole derivatives to second order for a number of selected local oscillators represented by internal coordinates. Higher-order force constants are calculated by numerical differentiation of second-order (harmonic) force constants obtained from standard quantum chemical methods such as Hartree-Fock or density functional theory. An anharmonic vibrational Hamiltonian is then generated and diagonalized. The representation of the dipole is then transformed into the eigenstate basis, resulting in transition dipole moments between all the eigenstates. Those together with the eigenstate energies are used to calculate nonlinear coherent signals applying the sum over states approach.[13]

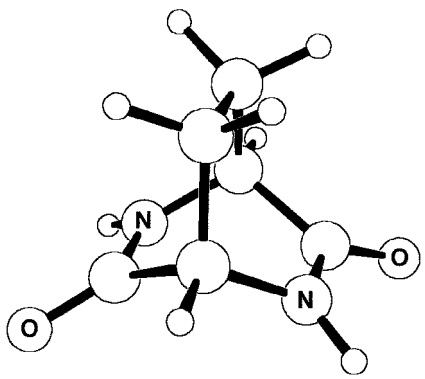

Scheme 1

[†]Present Addresses: Max-Born-Institut für Nichtlineare Optik und Kurzzeitspektroskopie, D-12489 Berlin, Germany.

Different coherent nonlinear techniques are classified by their phase matching conditions, four of them being independent.[1,13] In this contribution we analyze the effect of different polarization conditions on nonlinear 2D IR spectra generated in the $\mathbf{k}_I = -\mathbf{k}_1 + \mathbf{k}_2 + \mathbf{k}_3$ wavevector direction calculated for a model dipeptide, 2,5-diazabicyclo[2.2.2]-octane-3,6-dione (DABCODO, Scheme 1). DABCODO exists in a single and rather rigid bicyclic conformation, making it consistent with the approximations inherent in our calculations of the orientional part of the response function.[3]

Theory

The third order nonlinear polarization is a convolution of the response functions $R^{(3)}_{ijkl}$ and the three incoming pulsed laser fields E_n

$$P^{(3)}_i(\mathbf{r},t) = \int_0^\infty dt_1 \int_0^\infty dt_2 \int_0^\infty dt_3 R^{(3)}_{ijkl}(t_3,t_2,t_1) \times E_j(\mathbf{r},\tau_3 = t - t_3) E_k(\mathbf{r},\tau_2 = t - t_3 - t_2) \times E_l(\mathbf{r},\tau_1 = t - t_3 - t_2 - t_1), \quad (1)$$

where t_1 and t_2 are the delay times between the three pulses and t_3 is the time between the third pulse and the time t when the signal is detected. The third-order response functions $R^{(3)}_{ijkl}$ describe the microscopic behavior of the system under the influence of the laser pulses. In the sum over states approach they are given by

$$(R_1)_{ijkl}(t_3,t_2,t_1) = \sum_{a,b,c,d} P(a)\langle i_{cd} j_{bc} k_{ab} l_{da}\rangle \times \mu_{ab}\mu_{bc}\mu_{cd}\mu_{da} I_{dc}(t_3) I_{db}(t_2) I_{da}(t_1) \quad (2)$$

$$(R_2)_{ijkl}(t_3,t_2,t_1) = \sum_{a,b,c,d} P(a)\langle i_{cd} j_{bc} k_{da} l_{ab}\rangle \times \mu_{ab}\mu_{bc}\mu_{cd}\mu_{da} I_{dc}(t_3) I_{db}(t_2) I_{ab}(t_1) \quad (3)$$

$$(R_3)_{ijkl}(t_3,t_2,t_1) = \sum_{a,b,c,d} P(a)\langle i_{cd} j_{da} k_{bc} l_{ab}\rangle \times \mu_{ab}\mu_{bc}\mu_{cd}\mu_{da} I_{dc}(t_3) I_{ac}(t_2) I_{ab}(t_1) \quad (4)$$

$$(R_4)_{ijkl}(t_3,t_2,t_1) = \sum_{a,b,c,d} P(a)\langle i_{ab} j_{bc} k_{cd} l_{da}\rangle \times \mu_{ab}\mu_{bc}\mu_{cd}\mu_{da} I_{ba}(t_3) I_{ca}(t_2) I_{da}(t_1) \quad (5)$$

with the lineshape function in the homogeneous limit

$$I_{vv'}(t) = \theta(t)\exp(-i\Omega_{vv'}t - \Gamma_{vv'}t). \quad (6)$$

$\Omega_{vv'}$ are the transition frequencies between two vibrational eigenstates v and v'. $\Gamma_{vv'}$ is a homogenous dephasing linewidth, and $\mu_{vv'}$ are the corresponding transition dipole moments describing the coupling between the states. $\theta(t)$ is the Heavyside function and $P(a)$ is the thermal population of the initial state a determined by a Boltzmann distribution.

The orientational factors $\langle i_\alpha j_\beta k_\gamma l_\delta\rangle$ describe the polarization dependence of the response functions and are assumed to be decoupled from the vibronic dynamics. The indices $i, j, k, l \in \{x,y,z\}$ refer to the lab-frame components of the linearly polarized laser fields. The orientational factors correspond to fourth-rank tensors composed of 81 tensor elements.[14] For isotropic materials such as liquids, there are 21 nonvanishing elements in the orientational part of the third order response function, 3 of which are independent: $\langle z_\alpha z_\beta y_\gamma y_\delta\rangle$, $\langle z_\alpha y_\beta z_\gamma y_\delta\rangle$, and $\langle z_\alpha y_\beta y_\gamma z_\delta\rangle$. All other tensor components can be expressed in terms of these 3 independent elements. For example,

$$\langle z_\alpha z_\beta z_\gamma z_\delta\rangle = \langle z_\alpha z_\beta y_\gamma y_\delta\rangle + \langle z_\alpha y_\beta z_\gamma y_\delta\rangle + \langle z_\alpha y_\beta y_\gamma z_\delta\rangle. \quad (7)$$

Polarization conditions for four-wave mixing photon echo experiments have been examined by Hochstrasser.[3] The orientational factor for isotropic systems is given by

$$\langle i_\alpha j_\beta k_\gamma l_\delta\rangle = \frac{1}{30}[\langle\cos\theta_{\alpha\beta}\cos\theta_{\gamma\delta}\rangle \times (4\cos\theta_{ij}\cos\theta_{kl} - \cos\theta_{ik}\cos\theta_{jl} - \cos\theta_{il}\cos\theta_{jk}) + \langle\cos\theta_{\alpha\gamma}\cos\theta_{\beta\delta}\rangle(4\cos\theta_{ik}\cos\theta_{jl} - \cos\theta_{ij}\cos\theta_{kl} - \cos\theta_{il}\cos\theta_{jk}) + \langle\cos\theta_{\alpha\delta}\cos\theta_{\beta\gamma}\rangle \times (4\cos\theta_{il}\cos\theta_{jk} - \cos\theta_{ij}\cos\theta_{kl} - \cos\theta_{ik}\cos\theta_{jl})]. \quad (8)$$

Thus, the tensor components given in Eq. (7) can be expressed as

$$\langle z_\alpha z_\beta z_\gamma z_\delta\rangle = \frac{1}{15}(\langle\cos\theta_{\alpha\beta}\cos\theta_{\gamma\delta}\rangle + \langle\cos\theta_{\alpha\gamma}\cos\theta_{\beta\delta}\rangle + \langle\cos\theta_{\alpha\delta}\cos\theta_{\beta\gamma}\rangle) \quad (9a)$$

$$\langle z_\alpha z_\beta y_\gamma y_\delta\rangle = \frac{1}{30}(4\langle\cos\theta_{\alpha\beta}\cos\theta_{\gamma\delta}\rangle - \langle\cos\theta_{\alpha\gamma}\cos\theta_{\beta\delta}\rangle - \langle\cos\theta_{\alpha\delta}\cos\theta_{\beta\gamma}\rangle) \quad (9b)$$

$$\langle z_\alpha y_\beta y_\gamma z_\delta\rangle = \frac{1}{30}(-\langle\cos\theta_{\alpha\beta}\cos\theta_{\gamma\delta}\rangle - \langle\cos\theta_{\alpha\gamma}\cos\theta_{\beta\delta}\rangle + 4\langle\cos\theta_{\alpha\delta}\cos\theta_{\beta\gamma}\rangle) \quad (9c)$$

$$\langle z_\alpha y_\beta z_\gamma y_\delta\rangle = \frac{1}{30}(-\langle\cos\theta_{\alpha\beta}\cos\theta_{\gamma\delta}\rangle + 4\langle\cos\theta_{\alpha\gamma}\cos\theta_{\beta\delta}\rangle - \langle\cos\theta_{\alpha\delta}\cos\theta_{\beta\gamma}\rangle) \quad (9d)$$

In this work, calculations are performed in the time-domain and the pulse envelopes are introduced approximately by assuming the quasi impulsive limit; all the applied fields are taken to be delta functions so that the integrations over time intervals (Eq. 1) can be eliminated and the signal is directly proportional to the nonlinear response function. Frequency-selective excitation is accounted for by defining a finite rectangular pulse bandwidth (± 100 cm^{-1}). Transitions within the frequency range of the carrier frequencies and the bandwidth are resonant, whereas all other Liouville space pathways are neglected, a manual application of the rotating

wave approximation.

We report logarithmic two-dimensional absolute value plots of the complex signals after Fourier transformation with respect to either t_1 and t_3

$$S_{ijkl}(\omega_3, t_2, \omega_1) = \int_{-\infty}^{\infty} dt_3 \int_{-\infty}^{\infty} dt_1 R^*_{ijkl}(t_3, t_2, t_1) \times \exp(-i\omega_3 t_3 - i\omega_1 t_1) \quad (10)$$

or similarly t_2 and t_3

$$S_{ijkl}(\omega_3, \omega_2, t_1) = \int_{-\infty}^{\infty} dt_3 \int_{-\infty}^{\infty} dt_2 R^*_{ijkl}(t_3, t_2, t_1) \times \exp(-i\omega_3 t_3 - i\omega_2 t_2). \quad (11)$$

Results and Discussion

We investigate the dipeptide model system DABCODO because of its relatively rigid structure and its small size which allows the use of high-level quantum chemistry calculations. We applied density functional theory at the B3LYP/6-31G(d,p) level,[15-18] as implemented in Gaussian 98,[19] to optimize the structure and calculate harmonic force constants with respect to internal coordinates. Anharmonic force constants were calculated for the subspace of 6 local vibrational modes, the C=O, N-H and C-N stretches of the two peptide bonds. An effective exciton Hamiltonian constructed in a basis state manifold of up to 10 excitation quanta was diagonalized and resulted in a total of 2153 eigenstates.[12]

Spectra are simulated in the frequency range of the symmetric (*s*) and antisymmetric (*a*) C=O stretching vibrations, ν_s(C=O) = Ω_s = 1780.8 cm^{-1} and ν_a(C=O) = Ω_a = 1773.8 cm^{-1}. Anharmonic shifts of the overtones and combination bands are Δ_{ss} = 4.6 cm^{-1}, Δ_{aa} = 12.3 cm^{-1} and Δ_{as} = 16.9 cm^{-1}. We calculate signals for one-color experiments with carrier frequencies $\bar{\omega}_1 = \bar{\omega}_2 = \bar{\omega}_3$ = 1700 cm^{-1}. In the phase matching direction $\mathbf{k}_I = -\mathbf{k}_1 + \mathbf{k}_2 + \mathbf{k}_3$ the 3 Feynman diagrams R_2, R_3 and R_1^* contribute (Fig. 1).

All polarization conditions investigated here are summarized in Table 1. They are designed to eliminate certain groups of peaks, for instance diagonal or cross peaks, to improve resolution of specific peaks by removing overlaps with others.[3,8] Orientational factors are calculated using linear combinations of the 4 basic tensor elements (Eq. 7). Diagonal peaks (DP) result from the Feynman diagrams R_2 and R_3 when the 4 interactions are with the same mode, either ν_s(C=O) or ν_a(C=O); the corresponding Liouville space pathways are denoted ssss or aaaa, respectively (cf. Table 1). Cross peaks arise from interactions with different modes, either asas/sasa (R_2) or aass/ssaa (R_3). In t_1 and t_3 the coherences for the R_2 and R_3 pathways are identical, so their intensities contribute to the same diagonal and cross peaks. This is not the case for the (ω_2, ω_3) dimensions: diagonal peaks at ($\omega_2 = 0$) arise from one R_2 pathway but two R_3 pathways, while cross peaks at ($\omega_2 = \Omega_s - \Omega_a, \Omega_s$) and

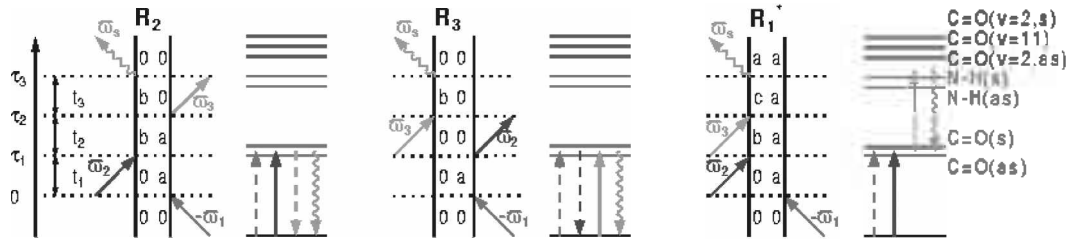

Figure 1. $\mathbf{k}_I = -\mathbf{k}_1 + \mathbf{k}_2 + \mathbf{k}_3$: Feynman diagrams ($R_s = R_2 + R_3 - R_1^*$) and energy level schemes (dashed arrows: interaction from the right; solid arrows: interaction from the left; wavy arrows: signal pulse) for $\bar{\omega}_1 = \bar{\omega}_2 = \bar{\omega}_3$ = 1770 cm^{-1} (ν(C=O)).

Table 1. Polarization factors $\langle i_\alpha j_\beta k_\gamma l_\delta \rangle$

Tensor element	Polarization Configuration				Feynman pathways:[a] $\alpha\beta\gamma\delta$		
	i	*j*	*k*	*l*	DP (R_3,R_3) aaaa/ssss	CP (R_2) asas/sasa	CP (R_3) aass/ssaa
zzzz	0	0	0	0	1/5	1/15	1/15
zzyy	0	0	$\pi/2$	$\pi/2$	1/15	−1/30	2/15
zyzy	0	$\pi/2$	0	$\pi/2$	1/15	2/15	−1/30
zyyz	0	$\pi/2$	$\pi/2$	0	1/15	−1/30	−1/30
zyzy−zyyz	0	$\pi/2$	$-\pi/4$	$\pi/4$	0	1/6	0
zzyy−zyyz	0	$-\pi/4$	$\pi/2$	$\pi/4$	0	0	1/6
zzyy−zyzy	0	$-\pi/4$	$\pi/4$	$\pi/2$	0	−1/6	1/6
zzzz−3 zzyy	0	0	$\pi/3$	$-\pi/3$	0	−1/30	−1/3
zzzz−3 zyzy	0	$\pi/3$	0	$-\pi/3$	0	−1/3	−1/30
zzzz−3 zyyz	0	$\pi/3$	$-\pi/3$	0	0	1/6	1/6

[a]DP = diagonal peak, CP = cross peak, a = ν_{as}(C=O), s = ν_s(C=O).

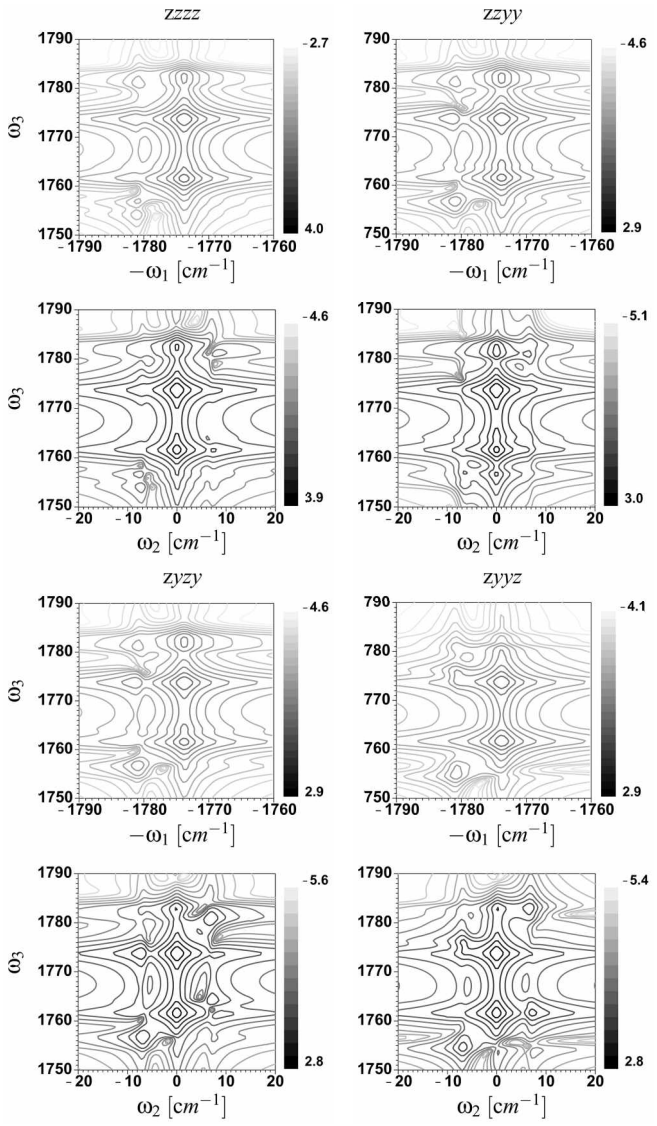

Figure 2. k_I: 2D magnitude spectra for the four basic tensor components where $\bar{\omega}_1 = \bar{\omega}_2 = \bar{\omega}_3 = 1770$ cm^{-1} (ν(C=O)), 1st and 3rd row: $\log|S(-\omega_1, t_2 = 0, \omega_3)|$, 2nd and 4th row: $\log|S(t_1 = 0, \omega_2, \omega_3)|$.

($\omega_2 = \Omega_a - \Omega_s, \Omega_a$) originate from single R_2 pathways.

DABCODO is C_2-symmetric, the 2 local C=O modes are degenerate and split symmetrically. Thus, the two transition dipole moments between the symmetric and antisymmetric C=O stretching modes (eigenstate picture) are orthogonal to each other.[3] This angle is needed to compute the orientational factors in Eq. (9) for the different Liouville space pathways underlying the diagonal and cross peaks (Table 1). The relative weights of the various Liouville space pathways also depend on the polarizations of the incident fields. The sign of the sum of Liouville pathways contributing to certain peaks may be directly observed in the real part of the spectra, however, we only show absolute values of the signals here.

Absolute value correlation plots for the 4 basic tensor components are shown in Figure 2. The spectra contain the complete set of diagonal, cross, overtone and combination band peaks. In the frequency range of the carbonyl stretching vibrations, a total of 10 and 16 peaks are seen in the ($-\omega_1, \omega_3$) and (ω_2, ω_3) plots, respectively. The sign of the sum of contributions to the cross peaks is negative for the zyyz polarization configuration in contrast to zzzz, zzyy and zyzy configurations.

The effect of taking linear combinations of different tensor elements is now easily evaluated from the linear combinations of the coefficients (see Table 1). It follows that diagonal peaks are eliminated by the linear combinations zyzy−zyyz, zzyy−zyyz and zzyy−zyzy as well as by zzzz−3zzyy, zzzz−3zyzy and zzzz−3zyyz. In addition, cross peaks vanish for the zzyy−zyyz combination.

The effects of forming the combinations zyzy−zyyz and zzyy−zyyz (Fig. 3) are similar in the ($-\omega_1, \omega_3$) dimensions: the diagonal peaks are eliminated and the cross peaks intensities are enhanced.

The relative intensities of the overtone peaks for the antisymmetric stretch at ($\Omega_a, \Omega_a - \Delta_{aa}$) are significantly reduced, whereas those of the combination bands at ($\Omega_a, \Omega_s - \Delta_{as}$) are increased, which improves the resolution of the combination bands by reducing their overlap with the stronger overtone peaks. The intensities of the peaks at (Ω_a, $2\Omega_s - \Omega_a - \Delta_{ss}$) are sligthly reduced but remain comparable in strength to the cross peak at (Ω_a, Ω_s) with which they overlap. Conversely, the overtone and combination band peak intensities for ($-\omega_1 = \Omega_s$) are all enhanced.

In contrast to the ($-\omega_1, \omega_3$) plots, the two combinations zyzy−zyyz and zzyy−zyyz differ considerably in the (ω_2, ω_3) dimensions. All diagonal peaks in which ($\omega_2 = 0$) vanish for the zyzy−zyyz combination, whereas the intensities of the cross peaks with ($\omega_2 = \Omega_a - \Omega_s$) and ($\omega_2 = \Omega_s - \Omega_a$) are identical to those in the ($-\omega_1, \omega_3$) plots. In contrast, the cross peaks at ($\Omega_s - \Omega_a, \Omega_s$) and ($\Omega_a - \Omega_s, \Omega_a$) cancel but the diagonal peaks survive for the zzyy−zyyz tensor combination.

Both diagonal and cross peaks which access only singly excited levels are entirely eliminated in the zzyy−zyzy combination. These peaks vanish due to destructive interferences between the Liouville space pathways (Table 1). The most intense peaks in these spectra appear at (Ω_a, $\Omega_s - \Delta_{as}$) and ($\Omega_s, \Omega_a - \Delta_{as}$). Thus, the resolution of the peaks at ($\Omega_a, 2\Omega_s - \Delta_{ss} - \Omega_s$) and ($\Omega_s, \Omega_s - \Delta_{ss}$) is improved. However, no clear improvement in resolution is gained in the (ω_2, ω_3) dimensions where all peaks persist.

In addition, the linear combinations zzzz−3zzyy, zzzz−3zyzy and zzzz−3zyyz (Figure 4) can also be employed to eliminate diagonal peaks from the ($-\omega_1, \omega_3$) spectra. The advantage of these combinations compared to zyzy−zyyz and zzyy−zyyz spectra is the greater overall intensity of the remaining peaks. As in the zzyy−zyzy combinations, no peaks are eliminated in the (ω_2, ω_3) plots.

In summary, we have simulated the effect of different polarization conditions on 2D IR spectra generated in the $\mathbf{k}_I = -\mathbf{k}_1 + \mathbf{k}_2 + \mathbf{k}_3$ wavevector direction. We demonstrated how diagonal and/or cross peaks can be eliminated from the spectra, facilitating the observation of peaks which are unresolved due to overlap with these stronger bands.

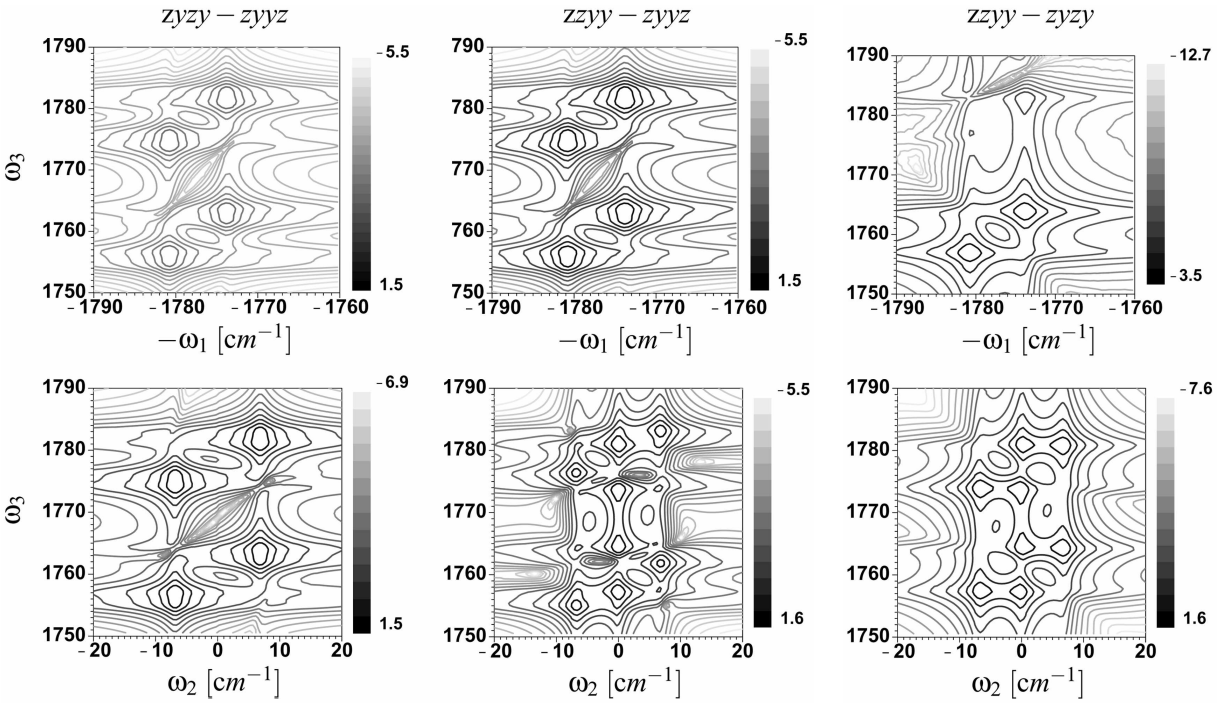

Figure 3. $\mathbf{k}_I$: 2D magnitude spectra for combinations of basic tensor components where $\bar{\omega}_1 = \bar{\omega}_2 = \bar{\omega}_3 = 1770$ cm^{-1} (ν(C=O)), upper panel: log|$S(-\omega_1, t_2 = 0, \omega_3)$|, lower panel: log|$S(t_1 = 0, \omega_2, \omega_3)$|.

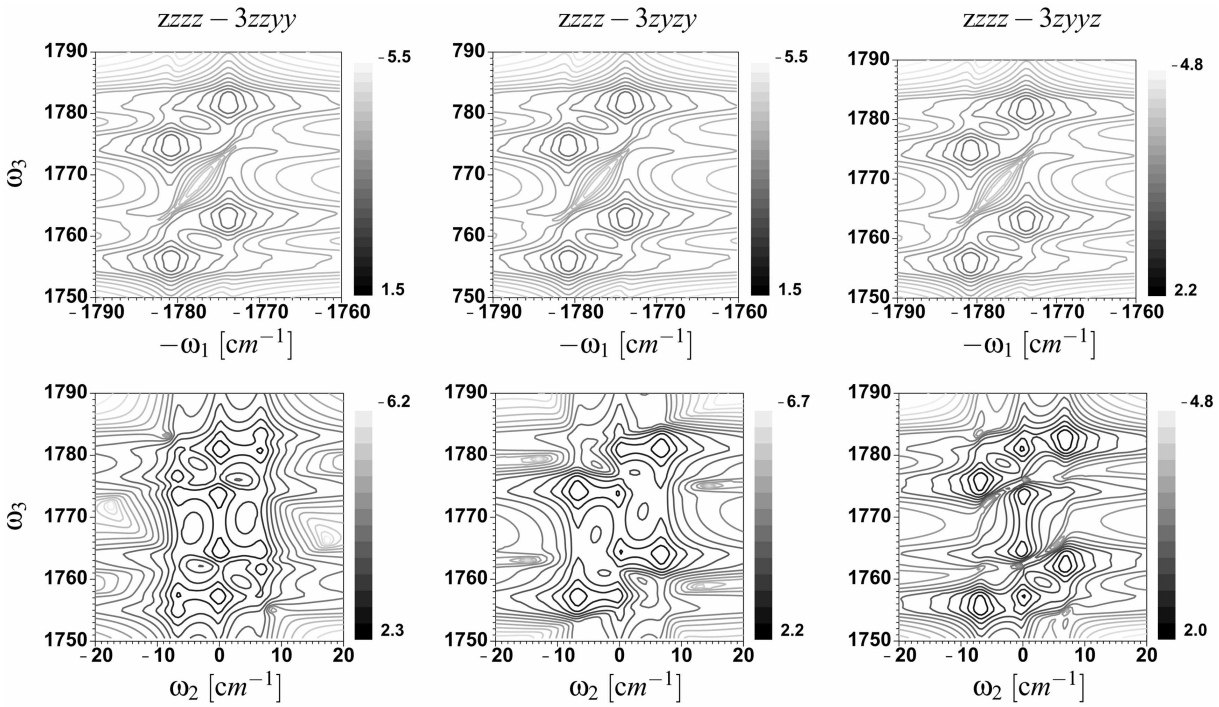

Figure 4. $\mathbf{k}_I$: 2D magnitude spectra for combinations of basic tensor components where $\bar{\omega}_1$ $\bar{\omega}_2$ $\bar{\omega}_3 = 1770$ cm^{-1} (ν(C=O)), upper panel: log|$S(-\omega_1, t_2 = 0, \omega_3)$|, lower panel: log|$S(t_1 = 0, \omega_2, \omega_3)$|.

Acknowledgments. We wish to thank Professor Thomas Elsässer for useful discussions. The support of The National Institutes of Health grant no. RO1 GM59230-01A2 and the National Science Foundation grant no. CHE-0132571 is gratefully acknowledged. J.D. would like to thank the Max-Kade foundation for financial support of his stay in Rochester.

References

1. Mukamel, S. *Annu. Rev. Phys. Chem.* **2000**, *51*, 691.
2. *Special Issue in Chem. Phys.*; Mukamel, S.; Hochstrasser, R., Eds.; 2001; vol. 135.
3. Hochstrasser, R. M. *Chem. Phys.* **2001**, *266*, 273.
4. Golonzka, O.; Tokmakoff, A. *J. Chem. Phys.* **2001**, *115*, 297.

5. Hamm, P.; Lim, M.; DeGrado, W. F.; Hochstrasser, R. M. *Proc. Natl. Acad. Sci.* U.S.A. **1999**, *96*, 2036.
6. Woutersen, S.; Hamm, P. *J. Phys. Chem. B* **2000**, *104*, 11316.
7. Zanni, M. T.; Gnanakaran, S.; Stenger, J.; Hochstrasser, R. M. *J. Phys. Chem. B* **2001**, *105*, 6520.
8. Zanni, M. T.; Ge, N.-H.; Kim, Y. S.; Hochstrasser, R. M. *Proc. Natl. Acad. Sci.* U.S.A. **2001**, *98*, 11265.
9. Ge, N.-H.; Hochstrasser, R. M. *Phys. Chem. Comm.* **2002**, *5*, 17.
10. Moran, A. M.; Dreyer, J.; Mukamel, S. *J. Chem. Phys.* **2003**, *118*, 1347.
11. Moran, A. M.; Park, S.-M.; Dreyer, J.; Mukamel, S. *J. Chem. Phys.* **2003**, *118*, 3651.
12. Dreyer, J.; Moran, A. M.; Mukamel, S. *J. Phys. Chem. B* **2003**, *107*, 5967.
13. Mukamel, S. *Principles of Nonlinear Optical Spectroscopy*; Oxford University Press: New York, Oxford, 1995.
14. *Molecular Light Scattering and Optical Activity*; Barron, L. D., Ed.; Cambridge University Press: Cambridge, 1982.
15. Lee, C.; Yang, R. G.; Parr, W. *Phys. Rev. B* **1988**, *37*, 785.
16. Miehlich, B.; Savin, A.; Stoll, H.; Preuss, H. *Chem. Phys. Lett.* **1989**, *157*, 200.
17. Becke, A. D. *J. Chem. Phys.* **1993**, *98*, 5648.
18. Hertwig, R. H.; Koch, W. *Chem. Phys. Lett.* **1997**, *268*, 345.
19. Frisch, M. J.; Trucks, G. W.; Schlegel, H. B.; Scuseria, G. E.; Robb, M. A.; Cheeseman, J. R.; Zakrzewski, V. G.; Montgomery, J. A.; Stratmann, R. E.; Burnat, J. C.; Dapprich, S.; Millam, J. M.; Daniels, A. D.; Kudin, K. N.; Strain, M. C.; Farkas, O.; Tomasi, J.; Barone, V.; Cossi, M.; Cammi, R.; Mennucci, B.; Pomelli, C.; Adamo, C.; Clifford, S.; Ochterski, J.; Petersson, G. A.; Ayala, P. Y.; Cui, Q.; Morokuma, K.; Malick, D. K.; Rabuck, A. D.; Raghavachari, K.; Foresman, J. B.; Cioslowski, J.; Ortiz, J. V.; Stefanov, B. B.; Liu, G.; Liashenko, A.; Piskorz, P.; Komaromi, I.; Gomperts, R.; Martin, R. L.; Fox, D. J.; Keith, T.; AlLaham, M. A.; Peng, C. Y.; Nanayakkara, A.; Gonzalez, C.; Challacombe, M.; Gill, P. M. W.; Johnson, B. G.; Chen, W.; Wong, M. W.; Andres, J. L.; Head-Gordon, M.; Replogle, E. S.; Pople, J. A. *Gaussian 98 (Revision A.9)*; Gaussian, Inc.: Pittsburgh, PA, 1988.